environmental microbiology

Environmental Microbiology (2022) **24**(4), 1887–1901 doi:10.1111/1462-2920.15921

Genotypic and phenotypic characterization of hydrogenotrophic denitrifiers

Clara Duffner[1,2] **Susanne Kublik**[2] **Bärbel Fösel**[2] **Åsa Frostegård**[3] **Michael Schloter**[1,2] **Lars Bakken**[3] **and Stefanie Schulz**[2*]

[1]*Chair of Soil Science, TUM School of Life Sciences Weihenstephan, Technical University of Munich, Freising, Germany.*

[2]*Research Unit Comparative Microbiome Analysis, Helmholtz Zentrum München, Neuherberg, Germany.*

[3]*Department of Chemistry, Biotechnology and Food Sciences, Norwegian University of Life Sciences, Ås, Norway.*

Summary

Stimulating litho-autotrophic denitrification in aquifers with hydrogen is a promising strategy to remove excess NO_3^-, but it often entails accumulation of the cytotoxic intermediate NO_2^- and the greenhouse gas N_2O. To explore if these high NO_2^- and N_2O concentrations are caused by differences in the genomic composition, the regulation of gene transcription or the kinetics of the reductases involved, we isolated hydrogenotrophic denitrifiers from a polluted aquifer, performed whole-genome sequencing and investigated their phenotypes. We therefore assessed the kinetics of NO_2^-, NO, N_2O, N_2 and O_2 as they depleted O_2 and transitioned to denitrification with NO_3^- as the only electron acceptor and hydrogen as the electron donor. Isolates with a complete denitrification pathway, although differing intermediate accumulation, were closely related to *Dechloromonas denitrificans*, *Ferribacterium limneticum* or *Hydrogenophaga taeniospiralis*. High NO_2^- accumulation was associated with the reductases' kinetics. While available, electrons only flowed towards NO_3^- in the *narG*-containing *H. taeniospiralis* but flowed concurrently to all denitrification intermediates in the *napA*-containing *D. denitrificans* and *F. limneticum*. The denitrification regulator RegAB, present in the *napA* strains, may further secure low intermediate accumulation. High N_2O accumulation only occurred during the transition to denitrification and is thus likely caused by delayed N_2O reductase expression.

Received 19 October, 2021; revised 20 January, 2022; accepted 20 January, 2022. *For correspondence. E-mail stefanie.schulz@helmholtz-muenchen.de; Tel. +49 89 3187 3054.

Introduction

Denitrification is the stepwise reduction of nitrate (NO_3^-) to dinitrogen (N_2), via the three intermediates nitrite (NO_2^-), nitric oxide (NO) and nitrous oxide (N_2O) (Zumft, 1997). The process is mainly performed by facultative anaerobic organo-heterotrophic prokaryotes (Rivett *et al*., 2008), which use the pathway to sustain respiratory metabolism under oxygen (O_2) limiting conditions. Such organisms are widespread among bacterial and archaeal phyla, but many of these lack one to three of the four genes coding for the four steps of denitrification, thus having incomplete denitrification pathways (Shapleigh, 2013; Graf *et al*., 2014). While denitrification is not desirable in agricultural soils because it reduces the amounts of NO_3^- available to crops, the process is beneficial in groundwater (GW) and wastewater treatment systems, where it removes excess NO_3^- that would otherwise deteriorate the water quality as well as the downstream environment (Rivett *et al*., 2008). Deliberate stimulation of denitrification in aquifers has been proposed as a method to eliminate NO_3^-, to secure drinking water quality. This can be achieved by injecting water with dissolved organic carbon, but the downside is massive growth of organo-heterotrophic bacteria, hence high bacterial load in the water (Matějů *et al*., 1992). This problem can be minimized, however, by injecting hydrogen (H_2) instead of organic carbon, thus stimulating denitrification by organisms that utilize H_2 as an electron donor and CO_2 as a carbon source (Karanasios *et al*., 2010). The reason is that litho-autotrophic denitrification sustained by the electron donor H_2 only yields 0.22–0.37 g cells for each g NO_3^--N reduced (Lee and Rittmann, 2003; Ghafari *et al*., 2009), compared to 0.6–0.9 g cells reported for organo-heterotrophic denitrification (Ergas and Reuss, 2001).

The ability to use H_2 as an electron donor for respiratory metabolism is widespread and the application of H_2 and its stimulating effect on denitrification has been proven in several laboratory experiments, bioreactors

and in *in situ* studies (Schnobrich *et al*., 2007; Chaplin *et al*., 2009; Wu *et al*., 2018). The conditions for hydrogenotrophic denitrification are highly selective (anoxic, inorganic carbon, H_2 as the sole electron donor and NO_x as the terminal electron acceptors) (Karanasios *et al*., 2010) and only a limited number of bacteria with this metabolism have been isolated, including strains belonging to the genera *Acidovorax*, *Paracoccus*, *Acinetobacter* and *Pseudomonas* (Szekeres *et al*., 2002; Vasiliadou *et al*., 2006). Additionally, several genera, including *Rhodocyclus*, *Sulfuricurvum*, *Sulfuritalea*, *Hydrogenophaga*, *Ferribacterium* and *Dechloromonas*, have been detected in 16S rRNA gene-based community analyses of hydrogenotrophic environments (Zhang *et al*., 2009; Zhao *et al*., 2011; Kumar *et al*., 2018b; Duffner *et al*., 2021). A recent community analysis microcosm experiment with nitrate-polluted aquifer material by Duffner *et al*. (2021) confirmed the low diversity of hydrogenotrophic denitrifiers (HDs). Only six amplified sequence variants (ASVs) were assigned to the genus *Dechloromonas*, and another unclassified *Rhodocyclaceae* ASV increased significantly in relative abundance during the incubations under an H_2 atmosphere. Additionally, the study suggested species- or even strain-level differences in the hydrogenotrophic denitrifying ability of *Dechloromonas*. In such low diversity communities, the contribution of single taxa to the overall observed metabolic process is strong. Previous studies have revealed a possible accumulation of the cytotoxic intermediate NO_2^- and the greenhouse gas N_2O during lithotrophic denitrification with H_2. Analysing the persistent or transient intermediate accumulation of individual HDs is therefore of interest, both for a basic understanding of the functioning of these bacteria and for their application in nitrate remediation of aquifers. A study by Vasiliadou *et al*. (2006) quantified the denitrification derived NO_2^- of some HDs, but the strains tested (*Acinetobacter* sp., *Acidovorax* sp. and *Paracoccus* sp.) do not seem to be dominant in aquifers, and the study was limited to non-gaseous NO_3^- and NO_2^-.

The reasons for incomplete denitrification and transient accumulation of intermediates have been studied for heterotrophic denitrifiers, and there are indications that multiple factors play a role, such as the absence of genes encoding the denitrification reductases, transcriptional regulation and post-translational processes determined by environmental conditions (Liu *et al*., 2013; Lycus *et al*., 2017). Such information on the regulation of denitrification and accumulation of intermediates for hydrogenotrophic denitrification is still lacking. We therefore isolated HDs from aquifer material and characterized their genotypes and phenotypes. The genomes were sequenced and screened for genes involved in hydrogenotrophic denitrification, which code for different denitrification reductase types, Rubisco forms (II, IA, IC) (Badger and Bek, 2008), hydrogenase groups (Greening *et al*., 2016) and denitrification regulators. Additionally, the 'denitrification regulatory phenotypes (DRPs)', a method established by Bergaust *et al*. (2011), were determined under litho-autotrophic conditions with H_2 as the sole electron donor and under organo-heterotrophic conditions with low concentrations of mixed carbon sources. The former was analyzed during the transition from aerobic respiration to denitrification and with cells that were already adapted to denitrification. This was done to differentiate between delayed gene expression and differential electron flow to the different denitrification reductases causing intermediate accumulation. As a control group, three closely related isolates of complete HDs assigned to *D. denitrificans* and *F. limneticum*, which were lacking the ability to reduce a significant amount of NO_3^- with H_2 as electron donor were subjected to the same genotypic and phenotypic characterization.

Results

Bacterial community composition in the original materials and enrichments

The bacterial community composition in the original sediment and GW materials as well as in the enrichments were analyzed via 16S rRNA gene amplicon sequencing. The rarefaction curves of the enrichment setups from the first (EI) and second (EII) enrichment procedure were all reaching a plateau within the subsampled range, indicating sufficient sequencing depth (Fig. S3). The number of ASVs in the original sediment samples was comparable between EI (1342) and EII (1863). However, there was a large difference for the original GW samples, as 2338 ASVs were detected in EI compared with 1202 in EII. The number of ASVs was much lower in the enrichment cultures, resulting in 1102 (EI)/646 (EII) ASVs in the highly active SED/GW enrichment and 144 (EI)/181 (EII) ASVs in the GW enrichment with slower reduction rates (Fig. S1B). The subsequent transfers of the enrichments to fresh nitrate-rich medium for one replicate of each setup further reduced the number of ASVs. In the original sediment and GW material, *Rhodocyclaceae* ASVs made up less than 0.5% relative abundance. Due to the enrichment, the relative abundance of *Rhodocyclaceae* ASVs was increased up to 32.2% in the transferred GW ($GW_{(t)}$) and up to 25.6% in the transferred sediment/GW ($SED/GW_{(t)}$) setups of EII (Fig. S4B). In contrast, in EI, the major increase in relative abundance was detected for *Burkholderiaceae* ASVs, which made up 79.8% in the transferred mineral medium and GW ($MM/GW_{(t)}$) enrichment setup (Fig. S4A).

Phylogenetic classification of the isolates

After separating the isolates on agar plates and determining their taxonomy, 48% of all Sanger sequenced isolates in EI were assigned to the family *Burkholderiaceae* and only 4% to *Rhodocyclaceae* (equivalent to one isolate). Contrary in EII, most of the isolates (26%) were assigned to the family *Rhodocyclaceae*. Most obtained *Rhodocyclaceae* isolates clustered with the genera *Dechloromonas*, *Ferribacterium* and *Quatrionicoccus* in the phylogenetic tree (Fig. S2), whereas most *Burkholderiaceae* isolates clustered with the genera *Hydrogenophaga*, *Acidovorax* and *Rhodoferax*. In total, 45 isolates, including isolated strains of all obtained families, were tested for their ability to reduce NO_3^- with H_2, but only some genera of *Rhodocyclaceae* and *Burkholderiaceae* showed this ability (Table S3). Of those isolates, which could reduce NO_3^- with H_2, the isolates $F76_{(HD)}$, $F77_{(HD)}$, $F128_{(HD)}$, $F132_{(HD)}$, $D110_{(HD)}$, $D6_{(HD)}$, $H3_{(HD)}$ and $H2_{(HD)}$ (Fig. 1; Table S3) were selected for further genotypic and phenotypic characterization because they display a range of phylogenetically closely related and diverse genera. Additionally, the three isolates, D98, Q100 and Q9, which lacked the ability of hydrogenotrophic denitrification but were closely related to the other *Rhodocyclaceae* HDs, were characterized alongside as a control group.

Most sequenced genomes were assembled into a single contig that could be circularized (Table S6). Only Q100 and $H3_{(HD)}$ had one or two additional smaller contigs respectively, which may be plasmids (Table S5). The completeness was above 99.2% and the contamination below 0.95% for all 11 sequenced genomes (Table S6).

For a genome-based phylogenetic classification, the number of reference genomes was low, especially for the genera *Ferribacterium* and *Quatrionicoccus*, as no sequenced genomes were available at NCBI at the time of analysis (www.ncbi.nlm.nih.gov/genome, March 2021). The phylogenetic classification, therefore, was mostly based on 16S rRNA gene comparisons. Based on the data obtained using TYGS (Meier-Kolthoff and Göker, 2019) (Table S8), isolates $F76_{(HD)}$, $F77_{(HD)}$, $F128_{(HD)}$ and $F132_{(HD)}$ were closest related to *Ferribacterium limneticum* CdA-1. While $F132_{(HD)}$ and $F128_{(HD)}$ shared highly similar genomes, $F76_{(HD)}$ and $F77_{(HD)}$ had a 16S rRNA gene identity of 99.4%, but their dDDH values only reached 60.8%, which did not allow a clear assignment to the same species. $D110_{(HD)}$ and $D6_{(HD)}$ were closest related to *Dechloromonas denitrificans* ED1. Both genomes were similar, with a dDDH value of 89.2%. A detailed comparison of the two isolates with *D. denitrificans* ED1 revealed 97.8% identity of 16S rRNA genes, a dDDH value of 34.7% and differences in the G + C content of less than 0.2%. This does not allow a clear assignment of the two isolates to the species *D. denitrificans*. Isolates $H3_{(HD)}$ and $H2_{(HD)}$ were both closest related to *Hydrogenophaga taeniospiralis* 2K1 according to the 16S rRNA gene sequences. However, a dDDH value of 37.5% and a G + C content difference of 1.5% between $H2_{(HD)}$ and *H. taeniospiralis* 2K1 suggested that this isolate belonged to a different species.

The isolate D98 of the control group was closest related to *D. denitrificans* ED1. However, while D98 clustered with *D. denitrificans* ED1 in the 16S rRNA

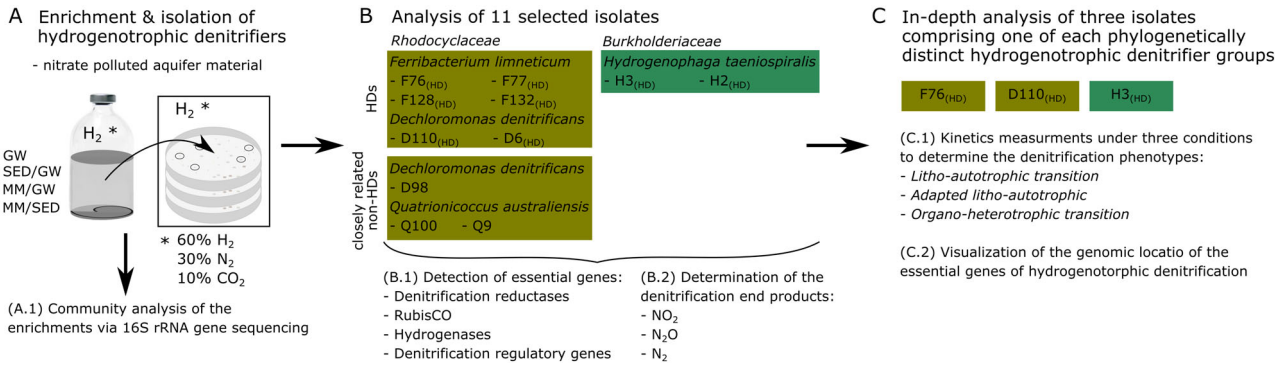

Fig. 1. Schematic overview of the experiments.
A. Initially, nitrate polluted aquifer material was incubated inside sealed vials in various setups with an H_2-containing atmosphere to enrich hydrogenotrophic denitrifiers and to isolate them on agar plates. (A.1) The community composition of the enrichments was additionally assessed by 16S rRNA gene amplicon sequencing.
B. Nine isolates of the families *Rhodocyclaceae* and two of the family *Burkholderiaceae* were selected for further (B.1) genotypic and (B.2) phenotypic analyses. Eight of the selected isolates were complete hydrogenotrophic denitrifiers (HDs) but the *Rhodocyclaceae* isolates also included three isolates which were closely related but were lacking the ability to denitrify with H_2 (non-HDs).
C. Finally, a sub-selection of three isolates, comprising one of each phylogenetically distinct hydrogenotrophic denitrifier groups ($F76_{(HD)}$, $D110_{(HD)}$, $H3_{(HD)}$) was analyzed in more depth. Therefore, (C.1) the denitrification phenotypes were determined under three different conditions and (C.2) the genomic location of hydrogenotrophic denitrifier genes was visualized.

gene-based phylogenetic tree (Fig. S6A), it clustered separately from all other isolated *Rhodocyclaceae* strains in the whole-genome sequence-based phylogenetic tree (Fig. S6B). The other two isolates of the control group, Q9 and Q100, were closest related to *Quatrionicoccus australiensis* Ben 117. The low dDDH values of 34.6% and 34.8% compared with the genome of *Q. australiensis* Ben 117 indicated that the isolates; however, belong to another species.

Phenotypes – intermediate accumulation during denitrification

The targeted isolation of bacteria revealed several complete HDs being capable of the complete reduction of NO_3^- to N_2 according to the endpoint analysis. These included eight isolates, which were assigned, based on their full 16S rRNA gene sequences, to the species *Ferribacterium limneticum* ($F76_{(HD)}$, $F77_{(HD)}$, $F128_{(HD)}$, $F132_{(HD)}$), *Dechloromonas denitrificans* ($D110_{(HD)}$, $D6_{(HD)}$) and *Hydrogenophaga taeniospiralis* ($H3_{(HD)}$, $H2_{(HD)}$) (Fig. 2A and B). Of the three closely related *Rhodocyclaceae* isolates (D98, Q100, Q9), which were analyzed as a control group, the two *Q. australiensis* isolates (Q100, Q9) reduced only NO_3^- to NO_2^-, while D98 did not reduce any nitrogen oxides (Fig. 2A and B). The pH at the endpoint measurements was on average significantly higher (0.11–0.18) in the incubations of the HDs compared with the non-inoculated incubations and the incubations with the isolates of the control group (lincon, $p \leq 0.009$) (Fig. S5A). The gas pressure was 0.125–0.151 bar lower in the incubations containing the HDs compared with the other incubations (lincon, $p \leq 0.009$) (Fig. S5B).

The DRPs were analyzed for a sub-selection of three HDs performing complete denitrification to N_2 ($F76_{(HD)}$, $D110_{(HD)}$ and $H3_{(HD)}$), which represent three phylogenetically distinct groups, under three conditions: *Litho-autotrophic transition*, *Adapted litho-autotrophic* and *Organo-heterotrophic transition* (Fig. 1). In the *Litho-autotrophic transition* experiment, the isolates $F76_{(HD)}$ and $D110_{(HD)}$, belonging to the family *Rhodocyclaceae*, displayed a continuous seamless transition to anaerobic respiration, i.e. the total electron flow continued to grow without any depression at the time of O_2 depletion (Fig. 3D and E). Furthermore, $F76_{(HD)}$ and $D110_{(HD)}$ initiated all denitrification steps simultaneously (Fig. 3A and B), as an electron flow was observed to all denitrification reductases from the onset of denitrification (Fig. 3D and E). The *H. taeniospiralis* isolate $H3_{(HD)}$ showed a similar seamless transition from aerobic respiration to NO_3^- reduction (no depression in total electron flow); however, the electron flow dropped substantially in response to NO_3^- depletion (Fig. 3F), which forced the cells to switch to nitrite reduction. The organism displayed a typical progressive onset of denitrification reactions (Liu *et al*., 2013) (Fig. 3C): initially, all electrons were flowing to NAR until all NO_3^- had been reduced to NO_2^-, before flowing to NIR, NOR and NOS (Fig. 3F). $F76_{(HD)}$ and $D110_{(HD)}$ differed significantly from $H3_{(HD)}$ in the O_2 concentration in the medium at the first appearance of NO: 6.9 μM (±0.37) O_2 for $F76_{(HD)}$, 8.1 μM (±1.75) O_2 for $D110_{(HD)}$ and 0.25 μM (±0.14) O_2 for $H3_{(HD)}$ (lincon, $p = 0.0127$) (Table 1 and S9). This contrast reflects the progressive onset of denitrification in $H3_{(HD)}$; however: in this strain, there was 8.3 μM (±1.6) O_2 in the liquid at the time when NO_2^- emerged. Thus, the three strains initiated anaerobic respiration at similar O_2 concentrations. Moreover, the relative growth rate (μ_{anoxic}/μ_{oxic}) was significantly lower for $H3_{(HD)}$ compared with $F76_{(HD)}$ (lincon, $p = 0.0121$) and $D110_{(HD)}$ (lincon, $p = 0.0343$) (Table 1 and S9). Even though $F76_{(HD)}$ and $D110_{(HD)}$ displayed a similar overall denitrification phenotype, they differed significantly in the transient NO_2^- accumulation of initial NO_3^- (lincon, $p = 0.0135$) (Table S9). $D110_{(HD)}$ accumulated on average 19.4% (±3.94) NO_2^- of the initial NO_3^-, whereas no NO_2^- accumulation was detected for $F76_{(HD)}$ (Table 1). Both, however, accumulated significantly less NO_2^- compared with 100% accumulated by the $H3_{(HD)}$ isolate (lincon, $p = 0.0124$) (Table 1 and S10). No significant differences between the three isolates were observed for the max. NO concentration in the medium and the maximum N_2O-N measured (t1way, $p = 0.24$ and 0.56) (Table S10). All isolates displayed a relatively high steady-state NO concentration, which ranged from 14.5–18.5 nM NO and a large variation in max. N_2O-N accumulation (Table 1).

In the *Organo-heterotrophic transition* experiment, we analyzed the DRPs with organic carbon as the electron donor and carbon source. The accumulated NO_2^- differed again significantly among the three isolates with the least NO_2^- accumulated in $F76_{(HD)}$ with 2.92% (±0.92), followed by $D110_{(HD)}$ with 9.54% (±0.81), and $H3_{(HD)}$ with 29.48% (±3.01) (Table 1). Especially for $H3_{(HD)}$, the transiently accumulated NO_2^- was significantly lower in the *Organo-heterotrophic transition* compared with the *Litho-autotrophic transition* experiment (t1way, $p = 0.0289$) (Table S11). Also, $D110_{(HD)}$ accumulated only approximately half of the NO_2^- measured during the H_2 transition experiment (Table 1). Contrary to the *Litho-autotrophic transition* experiments, the average max. steady-state NO differed significantly among the three isolates. It was significantly higher with 17.2 nM (±1.9) for isolate $H3_{(HD)}$, compared with 5.5 nM (±4.8) for $F76_{(HD)}$ (lincon, $p = 0.0212$) and 3.7 nM (±0.9) for $D110_{(HD)}$ (lincon, $p = 0.0004$) (Table S9). The max. accumulated N_2O-N was also significantly higher for isolate $H3_{(HD)}$ with 33.42% (±0.81) compared with 1.86%

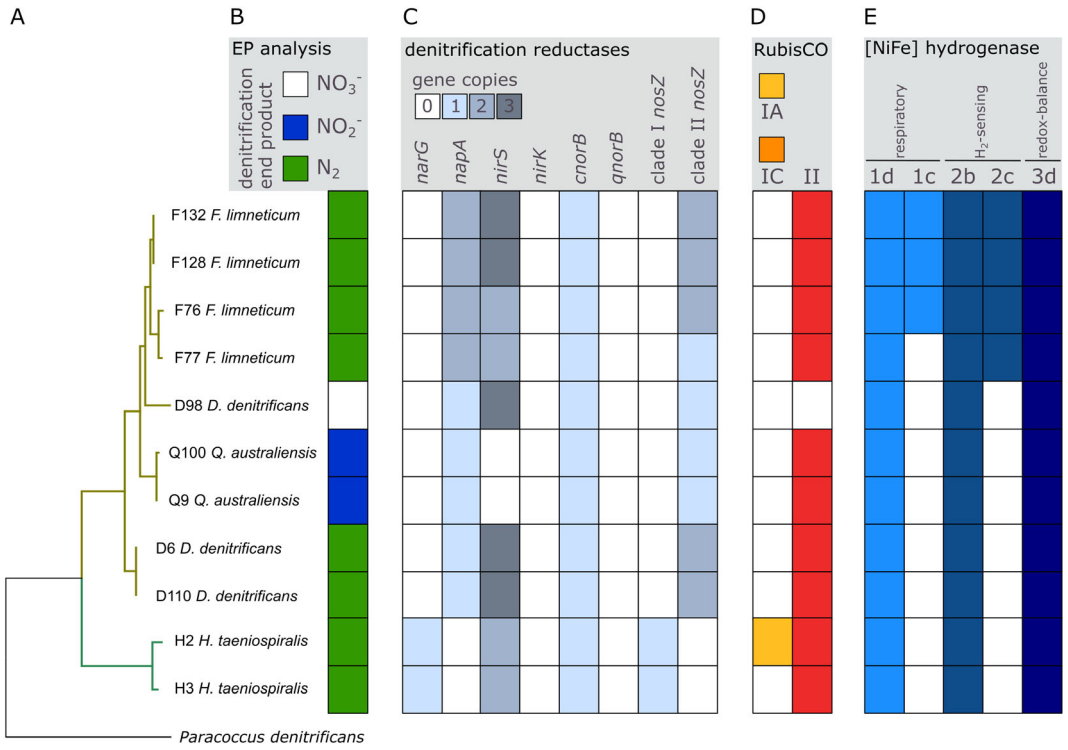

Fig. 2. (A) 16S rRNA gene-based maximum-likelihood phylogenetic tree of the 11 selected isolates from the genera *Rhodocyclaceae* (olive green) and *Burkholderiaceae* (dark green), as well as *Paracoccus denitrificans* (Y16927) as an outgroup. (B) Their denitrification end products were determined by measuring the changes in N-species after incubation in MM with H_2 as the sole electron donor and CO_2 as the sole carbon source. Furthermore, the type and copy number of (C) denitrification reductase, (D) RubisCO, and (E) hydrogenase genes detected in their sequenced genomes are displayed. White squares signify the absence of denitrification activity or the respective gene. Gas kinetics of the hydrogenotrophic denitrifier isolates (A) *F. limneticum* ($F76_{(HD)}$), (B) *D. denitrificans* ($D110_{(HD)}$) and (C) *H. taeniospiralis* ($H3_{(HD)}$) during the transition from aerobic respiration to denitrification in MM with H_2 as the sole electron donor are shown in the top panel. The period of denitrification is marked with a blue background, beginning at the appearance of detectable NO until all available nitrogen oxides had been reduced to N_2. [O_2], [NO_2^-], [NO], [N_2O] and [N_2] concentrations were quantified over time, while [NO_3^-] were extrapolated by subtracting the sum of N-oxides and N_2 from the initial [NO_3^-] concentration. The graphs are exemplary from one of several replicates, shown in Table 1. Calculated electron flow to the terminal oxidases (VeO_2) and the denitrification reductases (VeNAR/NAP, VeNIR, VeNOS) of isolates (D) $F76_{(HD)}$ ($n = 3$), (E) $D110_{(HD)}$ ($n = 6$), and (F) $H3_{(HD)}$ ($n = 6$) during the same experiment are shown in the bottom panel. The graphs show the average from several replicates (Table 1) and the standard deviations, which are large primarily due to temporal differences between replicate vials.

(±1.26) for $F76_{(HD)}$, and 0.82% (±1.49) for $D110_{(HD)}$ (both, lincon, $p \leq 0.0000$) (Table S9). However, it did not significantly differ from the N_2O-N accumulation in the H_2 transition experiment (Table S11). The concentration of dissolved O_2 at the appearance of detectable NO during the *Organo-heterotrophic transition* experiment was for isolates $F76_{(HD)}$ and $D110_{(HD)}$ approximately half of the average measured during the *Litho-autotrophic transition* experiment (t1way, both $p = 0.0289$) (Table 1 and S11).

In the *Adapted litho-autotrophic* experiment, the cells were already adapted to denitrification, i.e. equipped with a fully expressed denitrification proteome, with H_2 as the sole electron donor. In this experiment the max. accumulated NO_2^- still differed significantly among the three tested isolates. On average, $F76_{(HD)}$ transiently accumulated 0.02% (±0.01), $D110_{(HD)}$ 26.8% (±6.9) and $H3_{(HD)}$ 75.7% (±2.3) NO_2^- of the initial amount of NO_3^- added (Table 1). Unlike NO_2^-, which displayed a similar pattern in the *Adapted litho-autotrophic* and in the *Litho-autotrophic transition* experiment, the max. accumulated N_2O-N was much lower during the *Adapted litho-autotrophic* experiment (Table 1), even though the difference was again not significant due to the large variation among replicates.

During all three kinetics experiments, isolate $F76_{(HD)}$ displayed the least intermediate accumulation, followed by $D110_{(HD)}$, while $H3_{(HD)}$ displayed the largest intermediate accumulation, especially concerning that of NO_2^-.

Genotypes – genes of HDs

The hydrogenotrophic denitrifier isolates assigned to *F. limneticum* and *D. denitrificans* ($F76_{(HD)}$, $F77_{(HD)}$, $F128_{(HD)}$, $F132_{(HD)}$, $D110_{(HD)}$, $D6_{(HD)}$), were characterized by *napA* nitrate reductase genes and clade II *nosZ*

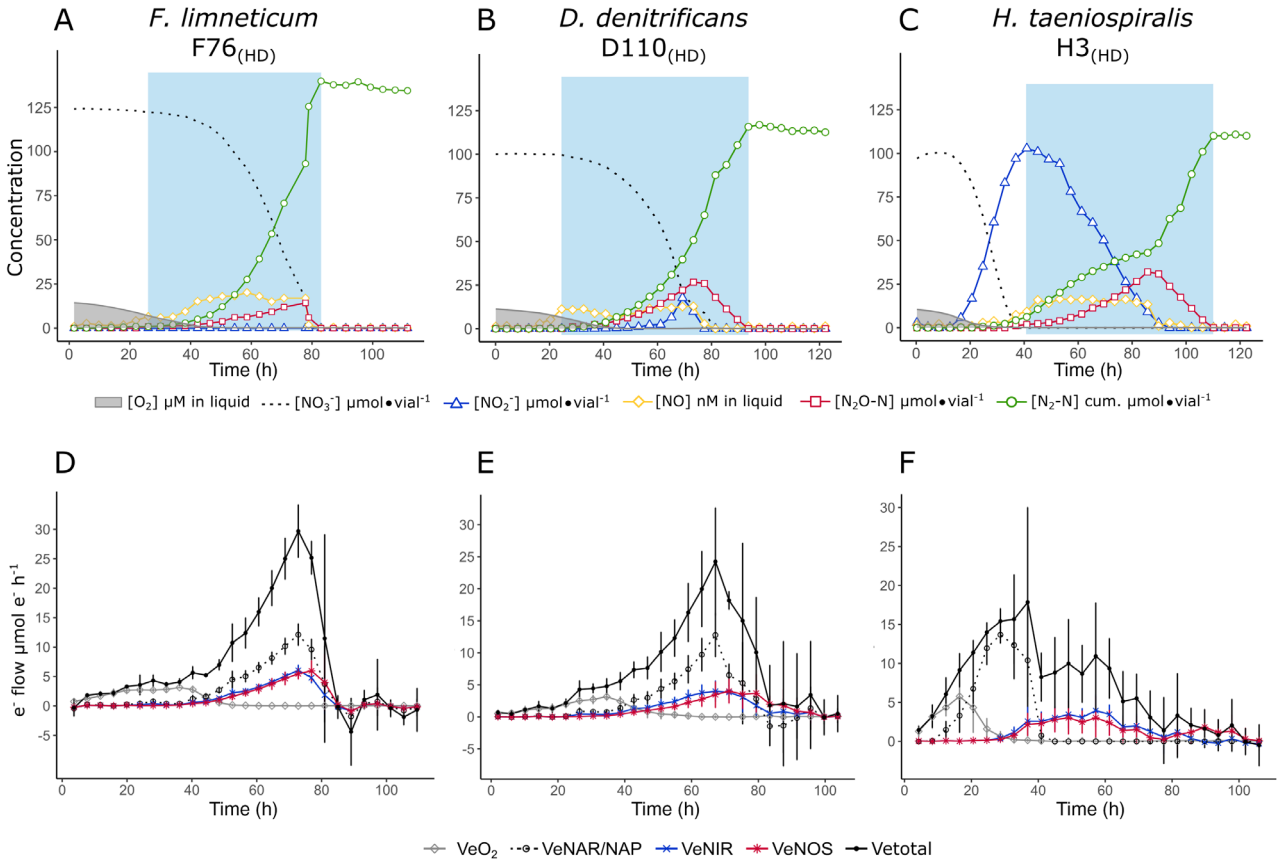

Fig. 3. Gas kinetics of the hydrogenotrophic denitrifier isolates (A) *F. limneticum* ($F76_{(HD)}$), (B) *D. denitrificans* ($D110_{(HD)}$) and (C) *H. taeniospiralis* ($H3_{(HD)}$) during the transition from aerobic respiration to denitrification in MM with H_2 as the sole electron donor are shown in the top panel. The period of denitrification is marked with a blue background, beginning at the appearance of detectable NO until all available nitrogen oxides had been reduced to N_2. [O_2], [NO_2^-], [NO], [N_2O] and [N_2] concentrations were quantified over time, while [NO_3^-] were extrapolated by subtracting the sum of N-oxides and N_2 from the initial [NO_3^-] concentration. The graphs are exemplary from one of several replicates, shown in Table 1. Calculated electron flow to the terminal oxidases (VeO_2) and the denitrification reductases (VeNAR/NAP, VeNIR, VeNOS) of isolates (D) $F76_{(HD)}$ ($n = 3$), (E) $D110_{(HD)}$ ($n = 6$), and (F) $H3_{(HD)}$ ($n = 6$) during the same experiment are shown in the bottom panel. The graphs show the average and standard deviation from several replicates, which are large primarily due to temporal differences between replicate vials.

nitrous oxide reductase genes (Fig. 2C). In contrast, the isolates assigned to *H. taeniospiralis* ($H3_{(HD)}$, $H2_{(HD)}$) harboured *narG* and clade I *nosZ* genes. All of them harboured *nirS* and *cnorB* rather than *nirK* and *qnorB* genes. For carbon assimilation, all complete hydrogenotrophic denitrifier isolates were equipped with a form II Rubisco gene (*cbbM*) (Fig. 2D), and several [NiFe]-hydrogenase genes (Fig. 2E) for H_2 oxidation. These hydrogenase genes comprised at least one group 1d respiratory hydrogenase gene, one group 2b H_2-sensing hydrogenase gene and one group 3d redox-balancing hydrogenase gene per genome. The *F. limneticum* isolates $F76_{(HD)}$, $F128_{(HD)}$ and $F132_{(HD)}$ additionally contained a group 1c respiratory hydrogenase gene and those isolates plus $F77_{(HD)}$, also harboured a group 2c H_2-sensing hydrogenase gene. All analyzed hydrogenotrophic denitrifier genomes contained the O_2-responsive regulator gene *fixL*, but the *D. denitrificans* and *F. limneticum* isolates, in contrast to the *H. taeniospiralis* isolates, were missing the two-component counterpart *fixJ* (Table S12). Instead, the genomes of the *Rhodocyclaceae* isolates contained one or multiple gene copies of the redox-sensing two-component system RegAB, which was not detected in the genomes of the two *H. taeniospiralis* isolates.

The location of these genes involved in hydrogenotrophic denitrification was analyzed for the genomes of the sub-selection, whose denitrification kinetics were also determined (Fig. 1). The analyzed genes were not confined to a certain region in either of the three genomes (Fig. S7). The denitrification operons in the genomes of $F76_{(HD)}$ and $D110_{(HD)}$ were less coherent compared with the genome of $H3_{(HD)}$. For example, one *nap* operon in $F76_{(HD)}$ and $D110_{(HD)}$ was fragmented into *napABC*, *napGH* and *napF* respectively. An extra *nap* operon in the $F76_{(HD)}$ genome was arranged as

Table 1. Basic characteristics of the denitrification phenotypes of the complete hydrogenotrophic denitrifiers *F. limneticum* ($F76_{(HD)}$), *D. denitrificans* ($D110_{(HD)}$) and *H. taeniospiralis* ($H3_{(HD)}$), as aerobically grown cells switched to denitrification while respiring H_2 only (*Litho-autotrophic transition*) or organic carbon only (*Organo-heterotrophic Transition*), and as the anaerobically H_2-respiring cells were given a second dose of NO_3^- and H_2 (*Adapted litho-autotrophic*).

Isolate	μ_{oxic}	μ_{anoxic}	μ_{anoxic}/μ_{oxic}	O_2 (μM) in liquid --> NO_2^-	O_2 (μM) in liquid --> NO	max. NO_2^- (% of initial NO_3^-)	max. NO (nM) in liquid	max. N_2O-N (% of initial NO_3^-)	*n*
Litho-autotrophic transition									
$F76_{(HD)}$	0.12 (±0.03)	0.10 (±0.01)	0.88 (±0.15)	nd[a]	6.9 (±0.4)	nd[a]	17.8 (±3.1)	7.1 (±4.6)	3
$D110_{(HD)}$	0.11 (±0.02)	0.10 (±0.02)	0.92 (±0.24)	1.5 (±1.4)	8.1 (±1.8)	19.4 (±3.9)	14.5 (±2.7)	13.3 (±11.3)	6
$H3_{(HD)}$	0.13 (±0.03)	0.03 (±0.01)	0.21 (±0.06)	8.3 (±1.6)	0.3 (±0.1)	100.1 (±13.7)	18.5 (±3.5)	18.3 (±15.5)	6
Adapted litho-autotrophic									
$F76_{(HD)}$	–	–	–	–	–	nd[a]	9.1 (±3.4)	2.4 (±4.1)	6
$D110_{(HD)}$	–	–	–	–	–	26.8 (±6.9)	16.1 (±4.3)	0.8 (±1.4)	3
$H3_{(HD)}$	–	–	–	–	–	75.7 (±2.3)	13.6 (±2.4)	0.01 (±0)	3
Organo-heterotrophic transition									
$F76_{(HD)}$	0.28 (±0.05)	0.16 (±0.04)	0.58 (±0.06)	10.3 (±0.6)	2.7 (±1.7)	2.9 (±0.9)	5.5 (±4.8)	1.9 (±1.3)	4
$D110_{(HD)}$	0.37 (±0.06)	0.29 (±0.06)	0.79 (±0.03)	8.2 (± 1.3)	1.7 (±0.8)	9.5 (±0.8)	3.7 (±0.9)	0.8 (±1.5)	4
$H3_{(HD)}$	0.18 (±0.10)	0.05 (±0.02)	0.35 (±0.20)	10.4 (±1.4)	0.3 (±0.1)	29.5 (±3.0)	17.2 (±1.9)	33.4 (±0.8)	4

napDAGHB. The *nar* genes of $H3_{(HD)}$, however, were organized all together as *narKGHJV*. Each analyzed genome contained multiple *nirS* gene copies in proximity, except for one *nirS* copy in the $D110_{(HD)}$ genome. Also, multiple copies of the accessory gene *nirM*, coding for cytochrome c551, were spread in all three genomes. The genes *norC* and *norB* clustered together close to *nirQ*, a synonym for *norQ*. While the *nos* operon genes of $H3_{(HD)}$ were located consecutively as *nosZ DFYL*, they were scattered among other genes in $F76_{(HD)}$ and $D110_{(HD)}$ (Fig. S7A and B). The *nos* genes of $F76_{(HD)}$ and $D110_{(HD)}$ were both accompanied by *regA*/*regB* genes.

Some of the above-specified genes were lacking in the genomes of the control group (D98, Q100, Q9). The two *Q. australiensis* isolates (Q100, Q9), which only reduced NO_3^- partly to NO_2^-, did not harbour any nitrite reductase gene, and D98, most closely related to *D. denitrificans*, did not harbour a RubisCO gene.

Discussion

Within this work bacteria that could denitrify with H_2 were isolated and characterized. The aim was to identify HDs with differing accumulation of intermediates, including NO_2^-, NO and N_2O, as well as to detect coherence between denitrification phenotypes, genetic properties and genome arrangement. The focus was on the genera *Dechloromonas* and its close relatives *Ferribacterium* and *Quatrionicoccus* from the family *Rhodocyclaceae*, as they had increased significantly in relative abundance in a recent microcosm experiment where H_2 was applied to stimulate lithotrophic denitrification with the aquifer material from the same location as used in this study (Duffner *et al*., 2021). The genus *Dechloromonas* has also been observed to thrive in other H_2-based environments, such as bioreactors (Zhang *et al*., 2009; Zhao *et al*., 2011) and microcosm experiments with GW and crushed rock material from a pristine aquifer (Kumar *et al*., 2018b). In the same experiments, the genus *Hydrogenophaga* was also detected. Indeed, in our study's second isolation, a large proportion of the isolates were assigned to the *Dechloromonas*, *Ferribacterium* and *Quatrionicoccus*, while in the first isolation, *Burkholderiaceae* isolates, mainly from the genera *Hydrogenophaga* and *Acidovorax*, were dominant. The different outcome could be due to high mineral nutrient concentrations in the MM that was used for the first isolation or due to the different sampling time points because seasonal differences in the bacterial community composition of aquifers are well-known (Chik *et al*., 2020). The multiple isolation of *D. denitrificans* and close relatives during the second isolation support their importance in hydrogenotrophic denitrification in oxic, nitrate-polluted oligotrophic aquifers (Duffner *et al*., 2021). While it is unclear which species prevails under which conditions, both *Dechloromonas* (and close relatives) and *Hydrogenophaga* obviously play an important role in hydrogenotrophic denitrification.

The significantly higher reduction in overpressure in the incubations with the HDs during the endpoint analysis compared to the control incubations confirms that the added H_2 and CO_2 were consumed by hydrogenotrophic bacteria. The increase in pH in the same incubations further indicates that denitrification occurred because denitrification uses protons to reduce NO_2^- to N_2 gas, increasing pH (Karanasios *et al*., 2010). The four isolates assigned to *F. limneticum* could all reduce NO_3^- to N_2 with H_2 as the electron donor, which was also the case for the closely related $D110_{(HD)}$ and $D6_{(HD)}$, belonging to the species *D. denitrificans*. The third group of complete HDs comprised the *Burkholderiaceae* isolates $H3_{(HD)}$ and $H2_{(HD)}$. While the first belonged to the species *H. taeniospiralis*, $H2_{(HD)}$ could be considered another species, based on the G + C content difference above 1%.

Genes for hydrogenotrophic denitrification

The genes coding for the dissimilatory nitrate reductase and nitrous oxide reductase differed between the *Rhodocyclaceae* isolates ($F76_{(HD)}$, $F77_{(HD)}$, $F128_{(HD)}$, $F132_{(HD)}$, $D110_{(HD)}$, $D6_{(HD)}$), which harboured *napA* and clade II *nosZ*, and the *Burkholderiaceae* isolates ($H3_{(HD)}$, $H2_{(HD)}$), which were characterized by *narG* and clade I *nosZ* genes. In conclusion, all complete HDs possessed denitrification reductases for all four steps, a form II Rubisco gene and three [NiFe] hydrogenase genes (group 1d, 2b and 3d). Thus, these genes are likely a prerequisite for hydrogenotrophic denitrification.

All detected hydrogenase genes in the analyzed hydrogenotrophic denitrifier genomes belonged to the [NiFe] class, which include the most common hydrogenases in bacteria (Vignais and Billoud, 2007). They harboured the O_2 tolerant group 1d respiratory [NiFe] hydrogenase (Greening *et al*., 2016), which is characteristic of many facultative anaerobic bacteria due to their frequent contact with O_2. Besides the respiratory hydrogenases, H_2-sensing and redox-balancing hydrogenases (Greening *et al*., 2016) were also detected. Of these, group 2b H_2-sensing [NiFe] hydrogenase controls hydrogenase expression, while the group 3d [NiFe] hydrogenase interconverts electrons between H_2 and NAD to adjust the redox state (Greening *et al*., 2016). Interestingly, only the *F. limneticum* isolates' genomes possessed extra hydrogenase genes (groups 1c and 2c). Moreover, CO_2 assimilation is an essential process of autotrophic hydrogenotrophic denitrification. Badger and Bek (2008) found that *Proteobacteria* may contain one or multiple RubisCO genes of the forms IA, IC and II, functioning at different concentrations of CO_2 and O_2. All investigated HDs possessed a form II Rubisco gene, which encodes a RubisCO version adapted to conditions with medium to high CO_2 and low or no O_2 (Badger and Bek, 2008). Thus, this is the only form that can assimilate CO_2 under anoxic conditions as encountered in the incubations.

Contrary to the findings of Yin *et al*. (2010), the genes of hydrogenotrophic denitrification did not cluster in close genome locations. Thus, their presence seems necessary, while their genomic location may vary. A plausible explanation for this observation is that operon proximity only occurs for operons whose encoding processes consistently work together, unlike denitrification, H_2 oxidation and CO_2 assimilation, which also function in combination with other metabolic pathways.

The closely related *Rhodocyclaceae* isolates, which lacked the ability to denitrify with H_2 (D98, Q100, Q9), lacked one of the mentioned genes which are likely a prerequisite of hydrogenotrophic denitrification: Q100 and Q9 lacked nitrite reductase gene, and D98 lacked a RubisCO gene. Additionally, D98 deviated phylogenetically from isolates $D110_{(HD)}$ and $D6_{(HD)}$, implying that D98 belonged to another species. The finding that all hydrogenotrophic denitrifying *Rhodocyclaceae* isolates either belonged to the species *D. denitrificans* or *F. limneticum*, and that the two isolates belonging to *Q. australiensis* and D98 of a so far not described species were incapable of hydrogenotrophic denitrification supports the finding of Duffner *et al*. (2021) that the ability for hydrogenotrophic denitrification among the family *Rhodocyclaceae* is species-specific.

Different hydrogenotrophic DRPs

Our data revealed that the *H. taeniospiralis* isolate $H3_{(HD)}$ differed significantly in multiple characteristics from the phenotypes of the *F. limneticum* isolate $F76_{(HD)}$ and the *D. denitrificans* isolate $D110_{(HD)}$. The most distinctive difference for isolate $H3_{(HD)}$ was the complete accumulation of NO_2^- until all NO_3^- had been reduced before continuing with further reduction steps, whereas isolates $F76_{(HD)}$ and $D110_{(HD)}$ initiated all denitrification steps simultaneously. This DRP of $H3_{(HD)}$ with a progressive onset of denitrification was also observed in several *Thauera* strains studied by Liu *et al*. (2013) as well as in another *Hydrogenophaga*, and a *Polaromonas* isolate studied by Lycus *et al*. (2017), with carbon as the electron donor. Like isolate $H3_{(HD)}$, the latter two are known to carry a *nar* gene, while isolates with the opposite phenotype, $F76_{(HD)}$ and $D110_{(HD)}$, harboured *nap* genes. Such a coherence between this distinct phenotype and the type of nitrate reductase has also been observed in recent studies by Gao *et al*. (2021) and Mania *et al*. (2020) for denitrifying *Bradyrhizobium* isolates. They also found that denitrifying *napA*-harbouring bradyrhizobia prefer N_2O reduction over NO_3^- reduction, while no such preference was detected in *narG*-carriers. This indicates that the electron pathway to the membrane-bound cytoplasmic nitrate reductase NarG competes better for electrons than the pathway to the periplasmic nitrate reductase NapA. The latter obtains electrons from NapC, a membrane-bound c-type cytochrome receiving electrons from the membrane-associated quinol pool, while NarG obtains electrons directly from the membrane-associated quinol pool (Shapleigh, 2013). The strong competition for electrons by the NarG pathway may prevent other denitrification reductases from receiving electrons when NO_3^- is still available, resulting in substantial NO_2^- accumulation like measured for $H3_{(HD)}$. The observation, that the transient NO_2^- accumulation did not differ significantly between the *Litho-autotrophic transition* and *Adapted litho-autotrophic* experiment for all tested isolates, further reasserts the hypothesis that the difference in NO_2^-

accumulation was due to differential electron flow rather than to differential gene expression. However, the occurrence of a *narG* gene cannot be the sole factor leading to 100% transient NO_2^- accumulation, as some *narG*-carrying bacteria, such as a *Pseudomonas* isolate in the study of Lycus *et al*. (2017), did not show any NO_2^- accumulation during denitrification with carbon. This could possibly be due to regulation at the transcriptional level (low transcription of *narG*). Contrary to transient NO_2^- accumulation, transient N_2O accumulation was on average considerably lower when the isolates were already equipped with a denitrification proteome (adapted to denitrification) compared with the transition phase, indicating that delayed *nos* gene expression caused most N_2O accumulation during the transition from aerobic respiration to denitrification. There was, however, considerable variation in transient N_2O accumulation between replicate experiments, also observed by Liu *et al*. (2013) with *Thauera* strains performing heterotrophic denitrification. The type of nitrous oxide reductase may influence the amount of N_2O accumulation as clade II NosZ enzymes have higher apparent N_2O affinity, higher biomass yield, and a more energy-efficient translocation mechanism compared with clade I NosZ (Yoon *et al*., 2016). Isolate $H3_{(HD)}$ also differed in this regard from $F76_{(HD)}$ and $D110_{(HD)}$, as it contained clade I *nosZ*, while the other tested strains harboured clade II.

The three analyzed HDs displayed a seamless transition from aerobic respiration to denitrification, i.e. without a substantial depression in electron flow rate at the transition from oxic to anoxic conditions. This was the case both with H_2 and carbon as the electron donor, implying that all cells, or at least the largest fraction of the cells, switched to denitrification due to anoxia unlike a phenomenon termed bet-hedging, observed by Lycus *et al*. (2017) for some denitrifying soil isolates. However, a drop in the total electron flow was observed in $H3_{(HD)}$ after nitrate depletion. This could either indicate that the organism expressed too little nitrite reductase to sustain the same high respiratory metabolism as during nitrate reduction or that only a fraction of the cells expressed nitrite reductase.

The denitrification phenotypes of $F76_{(HD)}$ and $D110_{(HD)}$ differed significantly between the oxic–anoxic transition under *Litho-autotrophic* and *Organo-heterotrophic* conditions. Litho-autotrophy led to an earlier onset of denitrification, as NO was detected at a significantly higher O_2 concentration. Also, both the oxic and anoxic growth rates were lower during the *Litho-autotrophic* compared to the *Organo-heterotrophic transition* experiment. Autotrophic growth requires much more energy to assimilate CO_2 (Albina *et al*., 2019) compared to heterotrophic growth. Consequently, cells grown on H_2 and CO_2 may switch earlier to denitrification to avoid entrapment in anoxia (Hassan *et al*., 2014). This difference in the O_2 concentration at the initiation of denitrification was not observed in $H3_{(HD)}$. However, the onset of NO_3^- reduction to NO_2^- occurred long before NO was detected, wherefore the estimated growth rate of $H3_{(HD)}$ was likely mostly based on NO_3^- reduction to NO_2^-. In the isolates $F76_{(HD)}$ and $D110_{(HD)}$ autotrophy additionally led to less balanced denitrification with higher transient accumulation of NO_2^-, NO and N_2O, indicating an influence of the electron donor H_2 on the proportionate expression of the respective reductase genes. In isolate $H3_{(HD)}$ this was only visible in the transient NO_2^- accumulation, which was significantly lower during *Organo-heterotrophic transition*.

The transcriptional regulation of denitrification differs largely among denitrifiers; however, the range of diversity is unknown as the regulation has mostly been studied in model organisms (e.g. *Paracoccus denitrificans*) (Gaimster *et al*., 2017; Lycus *et al*., 2017). Denitrification regulation comprises a network of regulators responding to intra- and extracellular signals such as NO, O_2, NO_3^- and NO_2^- concentrations as well as pH (Gaimster *et al*., 2017). An important sensor of decreasing O_2 concentrations and activator of denitrification is the RegAB redox-sensing two-component system, which was detected in all *Rhodocyclaceae* isolates. The *H. taeniospiralis* isolates; however, seemed to rely on the O_2-sensing two-component system FixLJ as their genomes harboured both genes. While FixL is directly activated by O_2 (Spiro, 2012), the membrane-associated RegB kinase indirectly responds to decreasing O_2 concentration as it is regulated by the redox state of the ubiquinone pool by non-catalytic equilibrium binding of ubiquinone (Wu and Bauer, 2010). The direct sensing of the ubiquinone redox state inside the denitrification respiratory membrane by RegAB may enable its carrier to react faster to changes in the electron availability inside the denitrification respiratory membrane and thus regulate the electron flow more efficiently. This could be a factor leading to a more balanced phenotype observed in the isolates $F76_{(HD)}$ and $D110_{(HD)}$ compared with $H3_{(HD)}$. In isolate $F76_{(HD)}$ extra hydrogenase genes were detected which may be connected to the even lower intermediate accumulation observed in $F76_{(HD)}$ compared with $D110_{(HD)}$.

Experimental procedures

Enrichment and isolation of HDs

Enrichment. Sediment and GW were sampled from a highly NO_3^- polluted oxic aquifer in the Hohenthann region in Southeast Germany (GPS: 48°42′01.2″N, 12°00′10.2″E). Location and sampling methods are

described in Duffner *et al*. (2021). Samples were stored at 4°C for 1 day until the enrichment incubations started. The used mineral medium (MM) was based on the 'multipurpose mineral medium' described by Widdel and Bak (1992). It contained separately autoclaved basal medium (without sulphate), 30 mM $NaHCO_3$ and 1.5–2 mM $NaNO_3$, as well as filter-sterilized 0.2% (vol./vol.) trace element solution SL-10 (Widdel and Pfennig, 1981; Widdel *et al*., 1983), 0.1% (vol./vol.) selenite tungsten solution (Widdel and Bak, 1992) and 0.1% (vol./vol.) vitamin solution (Balch *et al*., 1979). After autoclaving, all other components were added to the basal medium, and the pH was adjusted to 7.2 with 1 M HCl.

Approximately 100 ml of either only GW, sediment and groundwater (SED/GW), MM and groundwater (MM/GW) or MM and sediment (MM/SED), containing approximately 1.3 mM (70 mg L^{-1}) $NaNO_3$, were incubated inside 200 ml vials sealed with a rubber septum and an aluminium crimp cap. The crimped vials were sparged with a gas mixture containing 60% H_2, 10% CO_2 and 30% N_2 at an approximate flow rate of 100 ml min^{-1}, until the O_2 content in the outflowing air was 0% according to a digital oximeter (Greisinger Electronic, Germany) (~0.5 mM $H_{2(aq)}$, 14°C). The sparged enrichments were incubated at 14°C–20°C, while samples were taken every 2–5 days to monitor the NO_3^- and NO_2^- concentrations spectrophotometrically. NO_3^- was quantified according to Velghe and Claeys (1985), and NO_2^- according to Tsikas *et al*. (1997). Once all NO_3^- and NO_2^- had been reduced, which took between 6 and 46 days depending on the initial material (Fig. S1B), isolation from the enrichments was initiated. For one replicate per treatment 10% (vol./vol.) were transferred to fresh MM or 0.2 μm filtered/autoclaved GW once all NO_3^- had been reduced. This was done three times before the isolation.

Bacterial community analysis of the enrichments. Two milliliters (SED/GW, MM/SED) or 10 ml (GW, MM/GW) of the final enrichments were pelleted and frozen for bacterial community analysis. Additionally, original sediment and the material collected on a 0.22 μm filter of 3 L GW of each sampling was analyzed. DNA was extracted using the NucleoSpin Soil Kit (Macherey Nagel, Germany) with buffer SL2 and 30 s at 5.5 m s^{-1} bead beating. A negative extraction control was run alongside the samples. The 16S rRNA gene amplicon sequencing library preparation, the Illumina MiSeq sequencing and data processing were conducted as described in Duffner *et al*. (2021), with the exception that the primer pair 515F (Parada *et al*., 2016) and 806R (Apprill *et al*., 2015) suggested by the Earth Microbiome Project (V4 region), was used (Walters *et al*., 2016). The demultiplexed reads were processed using the QIIME2 and the DADA2 plugin (Bolyen *et al*., 2019), setting the N-terminal trimming to 10 bp and the C-terminal trimming to 270 bp for the forward and to 200 bp for the reverse reads. After denoising (Table S1), on average 70.6% of the reads remained for the enrichments, whereas only 53.1% of the reads remained for the original sediment and GW samples. Singleton reads from domains other than bacteria, and ASVs with more than nine reads in the negative extraction control were removed. The datasets were subsampled to the minimum number of reads per sample, 35 921 (EI) and 28 584 (EII), using the vegan package (v.2.5–7) (Oksanen *et al*., 2019) included in the R project (v.4.0.3) (Team, 2019). The rarefaction curves were generated using the vegan package, and the stacked bar plots with the phyloseq package (v.1.34.0) (McMurdie and Holmes, 2013). The amplicon sequences have been deposited in the Sequence Read Archive repository under the BioSample accession numbers SAMN19613689–SAMN19613703 as part of the BioProject PRJNA727717.

Isolation. The enrichments were serially diluted (10^{-2}–10^{-4}) upon depletion of the given nitrate. 100 μl of the dilutions were plated on MM agar plates, prepared with 1.5% (wt./vol.) purified agar (Oxoid Thermo Fisher, USA), under a laminar flow. The agar plates were incubated in anoxic pots flushed for approximately 1 h with the H_2-containing gas mixture. The anoxic pots were incubated for approximately 6 weeks at 14°C–20°C. In total 300 colonies were picked and secured in a colony library on agar plates. A large portion of the grown colonies was less than 0.5 mm in diameter, white/transparent and circular with a smooth edge, similar to the colony morphology of *Dechloromonas denitrificans* (Horn *et al*., 2005). For phylogenetic identification of the isolates, a colony PCR was performed targeting the full 16S rRNA gene (described in Table S2). Forty-five isolates (Table S3; Fig. S2), including strains of the species *Dechloromonas denitrificans*, *Ferribacterium limneticum*, *Quatrionicoccus australiensis* and *Hydrogenophaga taeniospiralis*, were inoculated in MM with the same H_2 atmosphere as described above and tested for their ability to reduce NO_3^- while being incubated at 20°C for 5 days. Ten isolates could reduce at least 35% of the initial NO_3^- within the given time (Table S3). Thereof eight were used for further phenotypic and genotypic characterization. They are marked as HD (hydrogenotrophic denitrifier) hereafter. These isolates included four strains assigned to *F. limneticum* ($F76_{(HD)}$, $F77_{(HD)}$, $F128_{(HD)}$, $F132_{(HD)}$), two isolates assigned to *D. denitrificans* ($D110_{(HD)}$, $D6_{(HD)}$) and two isolates assigned to *H. taeniospiralis* ($H3_{(HD)}$, $H2_{(HD)}$) (Fig. 1). Additionally, three close relatives of *D. denitrificans* and *F. limneticum* (D98, Q100, Q9) without

denitrifying ability with H_2 were characterized as a control group.

Difference between EI and EII. The enrichment and isolation procedure was performed twice, termed EI and EII, to increase the number of isolates from the family *Rhodocyclaceae*. For EI groundwater and sediment was sampled on February 20th 2019, and for EII on October 18th 2019. For EI, two replicates were prepared for each setup (GW, SED/GW, MM/GW, MM/SED), whereas four replicates were prepared for each setup of EII (GW, SED/GW). A difference was that the enrichment setups with MM were omitted for EII, and the agar plates contained only 10% of the mineral and vitamin mixtures described above. Also, during EII the enrichments were transferred to 0.2 μm filtered and autoclaved GW instead of fresh MM like during EI. Details of the enrichment and isolation procedure of HDs are given in Fig. S1 and Table S4.

Sequencing and analysis of the isolates' genomes

The 11 selected isolates (Fig. 1) were grown in R2A medium aerobically at 30°C for 2–4 days up to late exponential phase and harvested to reach approximately 4.5×10^9 cells, as recommended by the QIAGEN Genomic-tip (20/G) procedure (QIAGEN, Germany) protocol. This anion-exchange-based DNA extraction method, ensuring minimal fragmentation, was performed according to the manufacturer's protocol. The obtained high-quality DNA was sheared to 9–14 kb long fragments and quantified using a fragment analyzer (Agilent Technologies, USA) and the large fragment DNF-492 Kit (Agilent Technologies). With a maximum total expected genome size of 33 Mb, multiplexed microbial libraries were generated with the SMRTbell Express Template Prep Kit 2.0 Part Number 101-696-100 v.6 (March 2020) (PacBio, USA) without size selection. The libraries were sequenced using PacBio SMRT cells with the Sequel System and 3.0 chemistry. The genomes were assembled by the HGAP4 pipeline (SMRT Link: 8.0.0.80529, PacBio) with a seed coverage of 30 (Table S5). The genome sequences were circularized using the Circlator software (Hunt *et al*., 2015), and the genome sequence quality was assessed with the CheckM software (Parks *et al*., 2015) (Table S6). The circularized genomes were annotated with Prokka (version 1.13) (Seemann, 2014) using a similarity e-value cut-off of $1e^{-05}$.

The taxonomy of the genomes was determined by the Type Strain Genome Server (TYGS), the successor of the Genome-to-Genome Distance Calculator, in August 2020 (Meier-Kolthoff and Göker, 2019; Meier-Kolthoff *et al*., 2021). Instead of using a restricted number of marker proteins, TYGS computes genome-scale phylogeny and infers species boundaries from closest type genome sequences. It thereby also calculates the digital DNA–DNA hybridisation (dDDH) and G + C content difference between two isolates and the closest type strain genomes, which was described as a more reliable method compared to average nucleotide identity for example (Meier-Kolthoff and Göker, 2019). Furthermore, the complete 16S rRNA gene sequences were extracted and the percentage identity with the most similar 16S RNA gene sequence was calculated. The species delineation for dDDH has been set as 70% (Meier-Kolthoff and Göker, 2019). The G + C content difference is also an indicator of phylogeny because it rarely exceeds 1% within species (Meier-Kolthoff *et al*., 2014). For 16S rRNA gene comparison, species delineation ranges between 97% and 98.5% in the literature, as there is no universal agreement on the species boundaries (Janda and Abbott, 2007).

Further focus was given on the identification of genes potentially involved in hydrogenotrophic denitrification, such as denitrification reductases (*napA*, *narG*, *nirS*, *nirK*, *qnorB*, *cnorB*, clade I and clade II *nosZ*), RubisCO, hydrogenase and denitrification regulatory genes (*fixL*, *fixJ*, *ntcA*, *nnr*, *regA*, *regB*, *narX*, *narL*, *narQ*, *narP*, *norR*, *nsrR*, *dnrD*, *dnrN*) (see Supplementary Materials 2).

For a sub-selection, including one isolate of each phylogenetically distinct hydrogenotrophic denitrifier group ($F76_{(HD)}$, $D110_{(HD)}$, $H3_{(HD)}$) (Fig. 1), the circular genomes were visualized using the DNAPlotter software (Carver *et al*., 2008) showing the location of the important hydrogenotrophic denitrifier genes. If these were in proximity, their gene neighbourhood was additionally plotted using Gene Graphics (Harrison *et al*., 2018).

The genome sequences with the BioSample accessions SAMN19030600–SAMN19030611 are deposited at NCBI under the BioProject PRJNA727717.

Analyses of the denitrification phenotypes

Incubation system. A robotized incubation system was used for all analyses of the denitrification endpoints and denitrification kinetics. The system, described in detail by Molstad *et al*. (2007) and Molstad *et al*. (2016), hosts up to 30 parallel stirred batch cultures (120 ml serum vials with Teflon coated magnetic bars, crimp sealed with butyl rubber membranes) in a water bath with constant temperature (18°C in our experiments). At intervals, the system samples the headspace by piercing the butyl rubber septa and drawing the sample by a peristaltic pump into injection loops. After injection, the pump is reversed, returning a volume of He (equal to the volume drawn) into the vial. The gas chromatographic system [CP4900 microGC, Varian (now Agilent Technologies)] measures O_2, N_2, N_2O, CO_2 and CH_4 with thermal conductivity

detectors, and a chemoluminescence NOx analyzer (Model 200A, Advanced Pollution Instrumentation, USA) is used to measure NO. Measurements of standard gas mixtures (25 ppmv NO in N_2, 150 ppmv N_2O and 1% CO_2 in He, 21% O_2 in N_2) alongside the incubations were used for calibration and capture dilution of the headspace gases and leakage (see Molstad *et al*., 2007 for details). A spreadsheet developed by Bakken (2021) was used to convert the chromatography output into gas concentrations in the headspace and in the liquid, and the rate of production/consumption of each gas for every time interval between two samples. For the incubations with H_2 in the headspace, there was a significant reduction of the headspace pressure, despite the system's return of He at each sampling, due to the consumption of both H_2 and CO_2. This necessitated inclusion of pressure depression into calculating the gas concentrations. Therefore, the kinetics and in particular the mass balances for these incubations were not as accurately determined as is described in Molstad *et al*. (2007). NO_3^- and NO_2^- liquid concentrations were determined as described in Lycus *et al*. (2017), in small liquid samples taken manually throughout the incubations.

Endpoint analysis. First, the denitrification end products of all 11 selected isolates (eight HDs and three control strains) were determined by an endpoint analysis, essentially as described by Lycus *et al*. (2017). The cultures were incubated anoxically in the presence of NO_3^-, NO_2^- and N_2O, which allowed us to determine if they had complete or only partial denitrification pathways and if they were able to convert all available electron acceptors to N_2 with H_2 as the sole electron donor. The endpoint analyses were performed in triplicate for all 11 isolates. Approximately 1 ml pre-culture at an optical density (OD_{600}) of 0.3 was centrifuged at 4400*g* for 5 min, washed twice with 1 ml MM and dispersed in 1 ml MM. Since $F77_{(HD)}$ did not grow aerobically in liquid culture, it had to be scratched from R2A agar plates and washed in MM (as the others). The washed inocula were injected into 120 ml vials with 50 ml MM containing 1.5 mM $NaNO_3$ and 0.5 mM $NaNO_2$. After He-flushing, the vials were injected with 40 ml H_2 $vial^{-1}$, 20 ml CO_2 $vial^{-1}$ and 1.4 ml N_2O $vial^{-1}$ ($\sim$50 μmol N_2O $vial^{-1}$). The resulting overpressure of approximately 725 mbar (C9555 pressure metre, Comark Instruments, UK) was not released, and the vials were incubated for a minimum of 10 days at 18°C and 120 rpm. First, the pressure in the vials was quantified, the pressure was then released, and the headspace gases were measured twice in the robotized incubation system. Furthermore, NO_3^- and NO_2^- concentrations were determined, and the pH was measured directly after opening each vial. The experiment included additional control vials with inoculum but without H_2 to check for potential denitrification by carry-over carbon. The cultures were streaked onto R2A plates before and after incubation to check for cell viability and contamination.

Denitrification kinetics. The kinetics were investigated for the sub-selection of strains including $F76_{(HD)}$, $D110_{(HD)}$ and $H3_{(HD)}$. The first two experiments investigated the DRPs of cells that were raised under strict oxic conditions (to avoid the synthesis of denitrification enzymes), and monitored for O_2, NO_2^-, NO, N_2O and N_2 as the batch cultures depleted O_2, switched to anaerobic respiration and converted NO_3^- to N_2. These transition experiments were conducted with cells growing litho-autotrophically (H_2, CO_2, no organic carbon) and with cells growing organo-heterotrophically (only organic carbon provided), thus in the following, we will call the two experiments *Litho-autotrophic transition* and *Organo-heterotrophic transition* respectively. The DRP revealed by these transition experiments effectively confounds the effects of regulation at the transcriptional and metabolic level. To inspect the regulation at the metabolic level for litho-autotrophic denitrification, we conducted a third experiment where we continued to monitor the *Litho-autotrophic transition* experiment vials after adding a new dose of $NaNO_3$. In the following, we will call this experiment *Adapted litho-autotrophic*.

Litho-autotrophic transition: Liquid pre-cultures were grown aerobically in the most suitable complex organic medium (R2A for $F76_{(HD)}$ and $D110_{(HD)}$, and 20% TSB for $H3_{(HD)}$; Table S7) to secure high cell density for the inoculation. When these had reached mid/late exponential phase, 20–50 ml of the culture was centrifuged at 8000*g* for 10 min, washed twice with 20 ml MM (to remove organic compounds) and finally dispersed in MM. The washed cells were used to inoculate the 120 ml vials (1 ml per vial) containing 50 ml MM with 2 mM $NaNO_3$. After He-flushing and the injection of 40 ml H_2 $vial^{-1}$ and 20 ml CO_2 $vial^{-1}$, the vials were placed in the robotized incubation system, where the overpressure was released before 0.6 ml O_2 gas was injected ($\sim$26.5 μmol O_2 $vial^{-1}$). The headspace gases were measured at 4 h intervals, and the experiment lasted ≥120 h. The initial NO_3^- concentration was determined, and NO_2^- was measured throughout the incubation, more frequently during its accumulation.

Organo-heterotrophic transition: This experiment was similar to the *Litho-autotrophic transition* experiment. The differences were that the washing of the inocula (1 ml pre-culture, $OD_{600} = 0.1$) was omitted, complex organic liquid media were used (R2A for $F76_{(HD)}$, $D110_{(HD)}$, and 20% TSB for $H3_{(HD)}$; Table S7) and the anoxic atmosphere contained only Helium as no H_2 and CO_2 gas

was injected to the headspace. Thus, CO_2 fixation and lithotrophic denitrification were excluded.

Adapted litho-autotrophic: At the end of the *Litho-autotrophic transition* experiments, the vials were re-flushed with He, injected with 40 ml H_2 $vial^{-1}$, 20 ml CO_2 $vial^{-1}$ (but no O_2) and 1 ml 0.1 M $NaNO_3$ (=100 μmol $vial^{-1}$, 2 mM in the liquid). The pressure was released, and the vials were monitored for NO_2^-, NO, N_2O and N_2 in the robotized incubation system until all NO_3^- had been recovered as N_2.

Control vials with the same setup but without inoculum were measured alongside the bacterial incubations to check for contamination and gas leakage. All experiments were performed with a minimum of three replicate (*n* stated in Table 1) for each isolate.

Because NO_2^- was measured manually at different time points than the gases, the concentrations at the time points of the gas sampling were estimated by interpolation, using the SRS1 Cubic Spline Software (http://www.srs1software.com). Additionally, the electron flow (μmol e^- h^{-1}) to terminal oxidases and the denitrification reductases (NAR/NAP, NIR, NOR, NOS) was calculated based on the gross rates of each step in denitrification. The graphs were compiled in R project (v.4.0.1) with the ggplot2 package (Wickham, 2016). Due to the small number of replicates, a robust one-way analysis of variance with trimmed means (t1way function) and the post hoc test lincon from the package WRS2 (Mair and Wilcox, 2019) was used to detect statistically significant differences in the basic denitrification phenotype characteristics between the three analyzed isolates and kinetics experiments. The *p*-values were adjusted for each experiment or experimental comparison with a Benjamini and Hochberg ('BH') correction (Benjamini and Hochberg, 1995). Adjusted *p*-values <0.05 were considered significant.

Conclusion

We isolated and characterized prevailing complete HDs, which belong to the species *F. limneticum*, *D. denitrificans* and *H. taeniospiralis*. The presence of all denitrification reductase genes, a form II RubisCO gene and a minimum of three [NiFe]-hydrogenase genes were identified as common features to denitrify with H_2 as electron donor and CO_2 as carbon source. The results indicated that under ideal conditions without an electron donor limitation and sufficient nutrients and vitamins available, a difference in transient NO_2^- accumulation can be attributed to a stronger electron flow to the nitrate reductase NarG than NapA rather than sequential gene expression. If hydrogenotrophic denitrifying communities are dominated by *napA* carrying bacteria, e.g. of the species *F. limneticum* and *D. denitrificans*, we would thus expect less NO_2^- accumulation compared with communities dominated by *narG*-carrying bacteria e.g. of *H. taeniospiralis*. Furthermore, the genome analysis indicated that the phenotypes with less transient NO_2^- accumulation were associated with the RegAB two-component system, which could improve the regulation of electron flow inside the denitrification respiratory membrane. As detected in the *F. limneticum* isolates, additional hydrogenase genes may have a similar effect and thereby minimize intermediate accumulation further. Based on the obtained data, the next step is to develop ways enabling targeted stimulation of complete HDs with the least intermediate accumulation.

Acknowledgements

Clara Duffner received funding by Deutsche Forschungsgemeinschaft (DFG) through TUM International Graduate School of Science and Engineering (IGSSE), GSC 81. We would like to thank the Nitrogen Group from NMBU for welcoming Clara Duffner as a guest researcher and for all the help and guidance she received from all members of the group. Also, we would like to thank Franz Buegger (Helmholtz Centre Munich) for his help in setting up the gas system and Gabriele Barthel (Helmholtz Centre Munich) for her insights on cultivating litho-autotrophic bacteria anaerobically.

References

Albina, P., Durban, N., Bertron, A., Albrecht, A., Robinet, J.-C., and Erable, B. (2019) Influence of hydrogen electron donor, alkaline pH, and high nitrate concentrations on microbial denitrification: a review. *Int J Mol Sci* **20**: 5163.

Apprill, A., McNally, S., Parsons, R., and Weber, L. (2015) Minor revision to V4 region SSU rRNA 806R gene primer greatly increases detection of SAR11 bacterioplankton. *Aquat Microb Ecol* **75**: 129–137.

Badger, M.R., and Bek, E.J. (2008) Multiple Rubisco forms in proteobacteria: their functional significance in relation to CO_2 acquisition by the CBB cycle. *J Exp Bot* **59**: 1525–1541.

Bakken, L. (2021) Spreadsheet for Gas Kinetics in Batch Cultures: KINCALC.

Balch, W.E., Fox, G.E., Magrum, L.J., Woese, C.R., and Wolfe, R.S. (1979) Methanogens: reevaluation of a unique biological group. *Microbiol Rev* **43**: 260–296.

Benjamini, Y., and Hochberg, Y. (1995) Controlling the false discovery rate: a practical and powerful approach to multiple testing. *J R Stat Soc B Methodol* **57**: 289–300.

Bergaust, L., Bakken, L.R., and Frostegård, Å. (2011) Denitrification regulatory phenotype, a new term for the characterization of denitrifying bacteria. *Biochem Soc Trans* **39**: 207–212.

Bolyen, E., Rideout, J.R., Dillon, M.R., Bokulich, N.A., Abnet, C.C., Al-Ghalith, G.A., *et al*. (2019) Reproducible, interactive, scalable and extensible microbiome data science using QIIME 2. *Nat Biotechnol* **37**: 852–857.

Carver, T., Thomson, N., Bleasby, A., Berriman, M., and Parkhill, J. (2008) DNAPlotter: circular and linear interactive genome visualization. *Bioinformatics* **25**: 119–120.

Chaplin, B.P., Schnobrich, M.R., Widdowson, M., Semmens, M.J., and Novak, P.J. (2009) Stimulating in situ hydrogenotrophic denitrification with membrane-delivered hydrogen under passive and pumped groundwater conditions. *J Environ Eng* **135**: 666–676.

Chik, A.H.S., Emelko, M.B., Anderson, W.B., O'Sullivan, K. E., Savio, D., Farnleitner, A.H., *et al*. (2020) Evaluation of groundwater bacterial community composition to inform waterborne pathogen vulnerability assessments. *Sci Total Environ* **743**: 140472.

Duffner, C., Holzapfel, S., Wunderlich, A., Einsiedl, F., Schloter, M., and Schulz, S. (2021) *Dechloromonas* and close relatives prevail hydrogenotrophic denitrification in stimulated microcosms with oxic aquifer material. *FEMS Microbiol Ecol* **97**: fiab004.

Ergas, S.J., and Reuss, A.F. (2001) Hydrogenotrophic denitrification of drinking water using a hollow fibre membrane bioreactor. *J Water Supply: Res Technol-Aqua* **50**: 161–171.

Gaimster, H., Alston, M., Richardson, D.J., Gates, A.J., and Rowley, G. (2017) Transcriptional and environmental control of bacterial denitrification and N_2O emissions. *FEMS Microbiol Lett* **365**: 1–8.

Gao, Y., Mania, D., Mousavi, S.A., Lycus, P., Arntzen, M.Ø., Woliy, K., *et al*. (2021) Competition for electrons favours N_2O reduction in denitrifying Bradyrhizobium isolates. *Environ Microbiol* **23**: 2244–2259.

Ghafari, S., Hasan, M., and Aroua, M.K. (2009) Effect of carbon dioxide and bicarbonate as inorganic carbon sources on growth and adaptation of autohydrogenotrophic denitrifying bacteria. *J Hazard Mater* **162**: 1507–1513.

Graf, D.R.H., Jones, C.M., and Hallin, S. (2014) Intergenomic comparisons highlight modularity of the denitrification pathway and underpin the importance of community structure for N_2O emissions. *PLoS One* **9**: 1–20.

Greening, C., Biswas, A., Carere, C.R., Jackson, C.J., Taylor, M.C., Stott, M.B., *et al*. (2016) Genomic and metagenomic surveys of hydrogenase distribution indicate H_2 is a widely utilised energy source for microbial growth and survival. *ISME J* **10**: 761–777.

Harrison, K.J., Crécy-Lagard, V.D., and Zallot, R. (2018) Gene graphics: a genomic neighborhood data visualization web application. *Bioinformatics (Oxford, England)* **34**: 1406–1408.

Hassan, J., Bergaust, L.L., Wheat, I.D., and Bakken, L.R. (2014) Low probability of initiating *nirS* transcription explains observed gas kinetics and growth of bacteria switching from aerobic respiration to denitrification. *PLoS Comput Biol* **10**: e1003933.

Horn, M.A., Ihssen, J., Matthies, C., Schramm, A., Acker, G., and Drake, H.L. (2005) *Dechloromonas denitrificans* sp. nov., *Flavobacterium denitrificans* sp. nov., *Paenibacillus anaericanus* sp. nov. and *Paenibacillus terrae* strain MH72, N_2O-producing bacteria isolated from the gut of the earthworm *Aporrectodea caliginosa*. *Int J Syst Evol Microbiol* **55**: 1255–1265.

Hunt, M., Silva, N.D., Otto, T.D., Parkhill, J., Keane, J.A., and Harris, S.R. (2015) Circlator: automated circularization of genome assemblies using long sequencing reads. *Genome Biol* **16**: 294.

Janda, J.M., and Abbott, S.L. (2007) 16S rRNA gene sequencing for bacterial identification in the diagnostic laboratory: pluses, perils, and pitfalls. *J Clin Microbiol* **45**: 2761–2764.

Karanasios, K.A., Vasiliadou, I.A., Pavlou, S., and Vayenas, D.V. (2010) Hydrogenotrophic denitrification of potable water: a review. *J Hazard Mater* **180**: 20–37.

Kumar, S., Herrmann, M., Blohm, A., Hilke, I., Frosch, T., Trumbore, S.E., and Küsel, K. (2018b) Thiosulfate- and hydrogen-driven autotrophic denitrification by a microbial consortium enriched from groundwater of an oligotrophic limestone aquifer. *FEMS Microbiol Ecol* **94**: fiy141.

Lee, K.-C., and Rittmann, B.E. (2003) Effects of pH and precipitation on autohydrogenotrophic denitrification using the hollow-fiber membrane-biofilm reactor. *Water Res* **37**: 1551–1556.

Liu, B., Mao, Y., Bergaust, L., Bakken, L.R., and Frostegård, Å. (2013) Strains in the genus *Thauera* exhibit remarkably different denitrification regulatory phenotypes. *Environ Microbiol* **15**: 2816–2828.

Lycus, P., Lovise Bøthun, K., Bergaust, L., Peele Shapleigh, J., Reier Bakken, L., and Frostegård, Å. (2017) Phenotypic and genotypic richness of denitrifiers revealed by a novel isolation strategy. *ISME J* **11**: 2219–2232.

Mair, P., and Wilcox, R. (2019) Robust statistical methods in R using the WRS2 package. *Behav Res Methods* **52**: 464–488.

Mania, D., Woliy, K., Degefu, T., and Frostegård, å. (2020) A common mechanism for efficient N_2O reduction in diverse isolates of nodule-forming bradyrhizobia. *Environ Microbiol* **22**: 17–31.

Matějů, V., Čižinská, S., Krejčí, J., and Janoch, T. (1992) Biological water denitrification—A review. *Enzyme Microb Technol* **14**: 170–183.

McMurdie, P.J., and Holmes, S. (2013) phyloseq: an R package for reproducible interactive analysis and graphics of microbiome census data. *PLoS One* **8**: e61217.

Meier-Kolthoff, J.P., Carbasse, J.S., Peinado-Olarte, R.L., and Göker, M. (2021) TYGS and LPSN: a database tandem for fast and reliable genome-based classification and nomenclature of prokaryotes. *Nucleic Acids Res* **50**: D801–D807.

Meier-Kolthoff, J.P., and Göker, M. (2019) TYGS is an automated high-throughput platform for state-of-the-art genome-based taxonomy. *Nat Commun* **10**: 2182.

Meier-Kolthoff, J.P., Klenk, H.-P., and Göker, M. (2014) Taxonomic use of DNA G+C content and DNA–DNA hybridization in the genomic age. *Int J Syst Evol Microbiol* **64**: 352–356.

Molstad, L., Dörsch, P., and Bakken, L.R. (2007) Robotized incubation system for monitoring gases (O_2, NO, N_2O N_2) in denitrifying cultures. *J Microbiol Methods* **71**: 202–211.

Molstad, L., Dörsch, P. & Bakken, L.R. (2016) Improved robotized incubation system for gas kinetics in batch cultures. Researchgate.

Oksanen, J., Blanchet, F.G., Friendly, M., Kindt, R., Legendre, P., McGlinn, D. *et al*. (2019) vegan: Community Ecology Package.

Parada, A.E., Needham, D.M., and Fuhrman, J.A. (2016) Every base matters: assessing small subunit rRNA primers for marine microbiomes with mock communities, time series and global field samples. *Environ Microbiol* **18**: 1403–1414.

Parks, D.H., Imelfort, M., Skennerton, C.T., Hugenholtz, P., and Tyson, G.W. (2015) CheckM: assessing the quality of microbial genomes recovered from isolates, single cells, and metagenomes. *Genome Res* **25**: 1043–1055.

R Core Team. (2019) *R: A Language and Environment for Statistical Computing*: Vienna, Austria: *R Foundation for Statistical Computing*.

Rivett, M.O., Buss, S.R., Morgan, P., Smith, J.W.N., and Bemment, C.D. (2008) Nitrate attenuation in groundwater: a review of biogeochemical controlling processes. *Water Res* **42**: 4215–4232.

Schnobrich, M.R., Chaplin, B.P., Semmens, M.J., and Novak, P.J. (2007) Stimulating hydrogenotrophic denitrification in simulated groundwater containing high dissolved oxygen and nitrate concentrations. *Water Res* **41**: 1869–1876.

Seemann, T. (2014) Prokka: rapid prokaryotic genome annotation. *Bioinformatics* **30**: 2068–2069.

Shapleigh, J. (2013) *The Prokaryotes: Prokaryotic Physiology and Biochemistry*. Berlin, Heidelberg: Springer.

Spiro, S. (2012) Nitrous oxide production and consumption: regulation of gene expression by gas-sensitive transcription factors. *Philos Trans R Soc B: Biol Sci* **367**: 1213–1225.

Szekeres, S., Kiss, I., Kalman, M., and Soares, M.I.M. (2002) Microbial population in a hydrogen-dependent denitrification reactor. *Water Res* **36**: 4088–4094.

Tsikas, D., Gutzki, F.-M., Rossa, S., Bauer, H., Neumann, C., Dockendorff, K., *et al*. (1997) Measurement of nitrite and nitrate in biological fluids by gas chromatography–mass spectrometry and by the Griess assay: problems with the Griess assay—solutions by gas chromatography–mass spectrometry. *Anal Biochem* **244**: 208–220.

Vasiliadou, I.A., Siozios, S., Papadas, I.T., Bourtzis, K., Pavlou, S., and Vayenas, D.V. (2006) Kinetics of pure cultures of hydrogen-oxidizing denitrifying bacteria and modeling of the interactions among them in mixed cultures. *Biotechnol Bioeng* **95**: 513–525.

Velghe, N., and Claeys, A. (1985) Rapid spectrophotometric determination of nitrate in mineral waters with resorcinol. *Analyst* **110**: 313–314.

Vignais, P.M., and Billoud, B. (2007) Occurrence, classification, and biological function of hydrogenases: an overview. *Chem Rev* **107**: 4206–4272.

Walters, W., Hyde, E.R., Berg-Lyons, D., Ackermann, G., Humphrey, G., Parada, A., *et al*. (2016) Improved bacterial 16S rRNA gene (V4 and V4-5) and fungal internal transcribed spacer marker gene primers for microbial community surveys. *mSystems* **1**: e00009-00015.

Wickham, H. (2016) *ggplot2: Elegant Graphics for Data Analysis*. New York: Springer-Verlag.

Widdel, F., and Bak, F. (1992) Gram-negative mesophilic sulfate-reducing bacteria. In *The Prokaryotes: A Handbook on the Biology of Bacteria: Ecophysiology, Isolation, Identification, Applications*, Balows, A., Trüper, H.G., Dworkin, M., Harder, W., and Schleifer, K.-H. (eds). Springer New York: New York, NY, pp. 3352–3378.

Widdel, F., Kohring, G.-W., and Mayer, F. (1983) Studies on dissimilatory sulfate-reducing bacteria that decompose fatty acids. *Arch Microbiol* **134**: 286–294.

Widdel, F., and Pfennig, N. (1981) Studies on dissimilatory sulfate-reducing bacteria that decompose fatty acids. *Arch Microbiol* **129**: 395–400.

Wu, J., and Bauer, C.E. (2010) RegB kinase activity is controlled in part by monitoring the ratio of oxidized to reduced ubiquinones in the ubiquinone pool. *mBio* **1**: e00272-00210.

Wu, J., Yin, Y., and Wang, J. (2018) Hydrogen-based membrane biofilm reactors for nitrate removal from water and wastewater. *Int J Hydrogen Energy* **43**: 1–15.

Yin, Y., Zhang, H., Olman, V., and Xu, Y. (2010) Genomic arrangement of bacterial operons is constrained by biological pathways encoded in the genome. *Proc Natl Acad Sci U S A* **107**: 6310–6315.

Yoon, S., Nissen, S., Park, D., Sanford, R.A., and Löffler, F. E. (2016) Nitrous oxide reduction kinetics distinguish bacteria harboring clade I NosZ from those harboring clade II NosZ. *Appl Environ Microbiol* **82**: 3793–3800.

Zhang, Y., Zhong, F., Xia, S., Wang, X., and Li, J. (2009) Autohydrogenotrophic denitrification of drinking water using a polyvinyl chloride hollow fiber membrane biofilm reactor. *J Hazard Mater* **170**: 203–209.

Zhao, H.P., Van Ginkel, S., Tang, Y., Kang, D.-W., Rittmann, B., and Krajmalnik-Brown, R. (2011) Interactions between perchlorate and nitrate reductions in the biofilm of a hydrogen-based membrane biofilm reactor. *Environ Sci Technol* **45**: 10155–10162.

Zumft, W.G. (1997) Cell biology and molecular basis of denitrification. *Microbiol Mol Biol Rev* **61**: 533–616.

Supporting Information

Additional Supporting Information may be found in the online version of this article at the publisher's web-site:

Appendix S1: Supplementary Information.